J. Fluid Mech. (1981), *vol.* 112, *pp.* 411–431
Printed in Great Britain

A finite-rate theory of quadratic resonance in a closed tube

By MICHAEL P. MORTELL
University College, Cork, Ireland
AND BRIAN R. SEYMOUR
Department of Mathematics and Institute of Applied Mathematics and Statistics, University of British Columbia, Vancouver, B.C., Canada

(Received 24 September 1980)

Shock waves have been observed travelling in a closed gas-filled tube when the gas is excited by a piston operating at half the fundamental frequency of the tube. Linear theory predicts a continuous periodic solution, while its first correction in a regular expansion is unbounded at such a quadratic resonant frequency. To take account of the intrinsic nonlinearity of travelling waves, a finite-rate theory of resonance is necessary. The periodic motion is then calculated from discontinuous solutions of a functional equation. Two of the three weak-shock conditions and the entropy condition are inherent in the functional equation, and hence the addition of the equal-area rule to fit shocks ensures uniqueness of the solutions.

1. Introduction

When a gas in a closed tube is driven by an oscillating piston whose frequency ω is a multiple of the fundamental frequency of the tube, ω_1, there is no bounded periodic motion within acoustic theory. Multiples of the fundamental frequency are the linear resonant frequencies, $\omega_j = j\omega_1$. The first correction to linear theory in a regular expansion in powers of the dimensionless piston amplitude ϵ is also unbounded at the *quadratic resonant frequencies*, $\Omega_n = \frac{1}{2}(2n+1)\omega_1$; see Zarembo (1967) or Mortell & Seymour (1979). Thus, when $\omega = \Omega_n$ the acoustic solution has frequency Ω_n and the quadratic nonlinearity then gives rise to a forcing term with frequency $2\Omega_n$, which is a linear resonant frequency. In the theory of ordinary differential equations this phenomenon is referred to as superharmonic resonance of order 2; see Nayfeh & Mook (1979). In this paper we extend the finite-rate theory of resonant acoustic oscillations, given in Seymour & Mortell (1980) for the linear resonance region, to frequencies in the quadratic resonance region.

It was shown in Mortell & Seymour (1979) that the problem of calculating finite-rate forced oscillations of a gas in a closed tube could be reduced to finding periodic solutions of a functional equation. Finite-rate oscillations occur when the piston frequency and amplitude are such that there is appreciable distortion in the wave form in travelling the length of the tube. This distortion is characterized by the similarity parameter $A = 2\pi(\gamma+1)\epsilon\omega^2$, where γ is the gas constant (1·4 for air). Any experiment can be associated with a point in the A–Δ plane, where $\Delta = 2(\omega - \omega_n)$ measures the detuning from a linear resonant frequency. The A–Δ plane is divided by a transition curve into a region in which continuous periodic solutions exist, and where they do not. Discontinuous solutions, corresponding to frequencies in the linear resonance region,

were constructed in Seymour & Mortell (1980). Here we construct discontinuous solutions corresponding to piston frequencies in the quadratic resonance region, $|\omega - \Omega_n| < \frac{1}{2}(\frac{1}{2} - \Delta_q(A))$. This is done by using the fixed points of order 2 of the functional equation, appropriate to quadratic resonance. Such a fixed point corresponds physically to a 'resonating wavelet' in the propagating signal; i.e. an amplitude in the wave form which completes two cycles in the tube in an odd multiple of the piston period. Fixed points of order 1, appropriate to linear resonance, correspond to wavelets which complete one cycle in a multiple of the piston period.

The character of solutions in the quadratic-resonance region depends strongly on the magnitude of A. In the small-rate region $A \ll 1$, the solution of the functional equation contains two discontinuities per period. These discontinuities, whose strengths are approximately equal and depend on the value of $\Delta - \Delta_q(A)$, are separated by half a period. When $\Delta < \Delta_q(A)$ the solutions are continuous. The signal shape in the small-rate region can be explicitly determined from a nonlinear ordinary differential equation which may be simply derived from the functional equation, as in §5. Shocks are not inherent in the small-rate differential-equation theory in which the signal propagates according to linear theory. As a consequence it does not yield a unique solution, even with the addition of the entropy condition to ensure that discontinuities are compressive. Small-rate quadratic-resonance solutions, based on the theory of Chester (1964) for linear resonance, have been given by Galiev, Ilgamov & Sodykov (1970) and Keller (1975).

In the finite-rate region, corresponding approximately to $A > 0{\cdot}1$, the solution of the functional equation contains at least two discontinuities per period. These are not of equal strength, are not equally spaced, and their number depends on $\Delta - \Delta_q(A)$. Now $\Delta = \Delta_q(A)$ does not correspond to the transition from discontinuous to continuous solutions. The functional equation admits discontinuous solutions which automatically satisfy two of the three weak shock conditions and the entropy condition. Consequently, the addition of the equal-area rule uniquely determines the discontinuous solutions.

Periodic motions containing shocks have been observed at frequencies in the quadratic-resonance region by Galiev *et al.* (1970) and Zaripov & Ilgamov (1976). For the experiments of Galiev *et al.* (1970), the similarity parameter was in the interval $0{\cdot}025 < A < 0{\cdot}05$ i.e. in the small-rate range $A < 0{\cdot}1$, and correspond to $\epsilon = 0{\cdot}0327$. In the experiments of Zaripov & Ilgamov (1976), the effective piston amplitude was $\epsilon = 0{\cdot}1244$, with A in the interval $0{\cdot}09 < A < 0{\cdot}19$.

The basic functional equation (2.9) gives a certain unity to the theory of nonlinear forced oscillations in a closed tube. It predicts the continuous motions away from the resonances, and the discontinuous motions in the various resonance regions. Equation (2.9) also arises in a number of problems in nonlinear dynamics, where it can exhibit chaotic, or stochastic, solutions, even though the governing equations are deterministic. The continuous solutions within the transition curve of the A–Δ plane are the KAM surfaces (Kolmogorov, Arnol'd and Moser), see Greene (1979). The chaotic solutions occur for those values of A and Δ for which the wave form will break in one cycle in the tube, see Mortell & Seymour (1980). It is interesting to note that the restricted three-body problem of celestial mechanics has been reduced to the study of an area-preserving mapping and that the problem of 'small divisors' has been resolved in this context, see Moser (1962).

2. Formulation

A column of gas, of length L in some reference state, is contained in a pipe which is closed at one end. At the other end there is a reciprocating piston. In terms of the variables $a_0 u$, $\rho_0 a_0^2 p$, Lx, $La_0^{-1}t$ it has been shown in Mortell & Seymour (1979) that, to first order, for the isentropic flow of an ideal gas

$$p = -f(\beta) - g(\alpha), \quad u = f(\beta) - g(\alpha), \tag{2.1}$$

where $$\alpha = \omega(t-x) - \omega M x g(\alpha), \quad \beta = \omega(t+x-1) + \omega M(x-1) f(\beta). \tag{2.2}$$

In equations (2.1) and (2.2), γp is the excess pressure ratio, u the (dimensionless) particle velocity, a_0 and ρ_0 are the reference sound speed and density, and $M = \frac{1}{2}(\gamma+1)$ where γ is the ratio of specific heats. The small-amplitude Lagrangian representations (2.1) and (2.2) are correct to $O(f^2, g^2)$.

The periodic piston displacement has the form $\epsilon \bar{h}(\omega t)$ where $\epsilon (\ll 1)$ and ω are the dimensionless piston amplitude and frequency, with $\bar{h}(y) = \bar{h}(y+1)$. Then the piston velocity, $h(y) = \epsilon\omega \bar{h}'(y)$, has unit period and zero mean value. Hence the boundary conditions have the form

$$u(0,t) = 0, \quad u(1,t) = h(\omega t). \tag{2.3}$$

The unknown Riemann invariants, f and g, in the representation (2.1) are determined from the boundary conditions (2.3). Eliminating g from equations (2.1)–(2.3) implies that f satisfies the functional equation

$$f(\eta) = f(s) + h(\eta), \quad \eta = s + 2\omega + 2\omega M f(s), \tag{2.4}$$

where g is related to f by $$g(\phi + \omega + \omega M f(\phi)) = f(\phi). \tag{2.5}$$

When the motion of the gas is periodic, f further satisfies $f(y) = f(y+1)$ and the mean condition $\int_0^1 f(y)\,dy = 0$; see Seymour & Mortell (1973).

Linear theory, which is recovered by setting $M = 0$ in equations (2.2), (2.4) and (2.5), fails to produce a bounded periodic solution when $\omega = \omega_j = \frac{1}{2}j$, $j = 1, 2, 3, \ldots$, *the linear resonant frequencies*. It is shown in Zarembo (1967) that the first correction to linear theory in a regular expansion in powers of ϵ has no bounded solution of unit period when

$$\omega = \Omega_n = \tfrac{1}{4}(2n+1), \quad n = 0, 1, 2, \ldots. \tag{2.6}$$

We call the frequencies $\omega = \Omega_n$ *quadratic resonant frequencies.*

Here we use the representation (2.1), (2.2), (2.4), (2.5) to describe the periodic motion of the gas for piston frequencies in a region containing a quadratic resonant frequency. We calculate periodic solutions f of equation (2.4) and hence determine the pressure and particle velocity in the tube from equations (2.1), (2.2) and (2.5). Defining

$$\Delta = \tfrac{1}{2} + 2(\omega - \Omega_n) = 2(\omega - \omega_n), \quad \omega_0 = 0, \tag{2.7}$$

$$F(y) = 2\omega M f(y) + \Delta, \quad H(y) = 2\omega M h(y), \tag{2.8}$$

equation (2.4) becomes

$$F(\eta) = F(s) + H(\eta), \quad \eta = s + F(s), \tag{2.9}$$

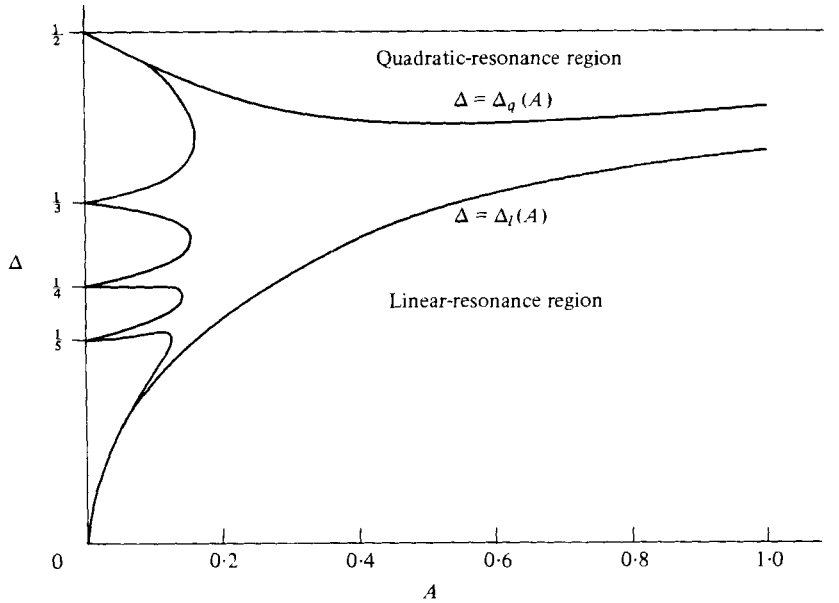

FIGURE 1. Transition curve in A–Δ plane, the linear-resonance region, $0 \leqslant \Delta \leqslant \Delta_l(A)$, and the quadratic-resonance region $\Delta_q(A) \leqslant \Delta \leqslant \frac{1}{2}$.

where F has unit period and satisfies the mean condition

$$\int_0^1 F(\eta)\, d\eta = \Delta. \tag{2.10}$$

Equations (2.9) and (2.10) are the basic equations from which the periodic oscillations for any frequency are determined. For the sinusoidal piston motion

$$h(\omega t) = 2\pi\epsilon\omega \sin(2\pi\omega t),$$

normally used in experiments,

$$H(\eta) = A \sin(2\pi\eta), \tag{2.11}$$

and hence the *similarity parameter* is $A = 4\pi M\epsilon\omega^2$. Clearly, specifying the experimental parameters (ϵ, ω, M) determines a unique point in the A–Δ plane. Similarly, given a solution curve F of equation (2.9) for a particular value of A, equation (2.10) uniquely associates a point in the A–Δ plane with F. Thus each solution curve F is associated with a single experiment for each mode number n.

Equations (2.9)–(2.11) were derived in Seymour & Mortell (1973), and were approximated by a nonlinear ordinary differential equation in the region $|\Delta| \ll 1$, $A \ll 1$. Continuous periodic solutions of equations (2.9)–(2.11) were constructed in Mortell & Seymour (1979). It was shown that the A–Δ plane is divided by a transition curve into regions where continuous periodic solutions can exist and where they do not; see figure 1. The transition curve is an even function of frequency about both the linear ($\Delta = 0$) and quadratic ($\Delta = \frac{1}{2}$) resonant frequencies, and hence the solutions for all frequencies can be represented in the strip $A \geqslant 0$, $0 \leqslant \Delta \leqslant \frac{1}{2}$. Equations (2.9) and (2.11) define a particularly simple area-preserving mapping, which has been named the 'standard mapping' by Chirikov (1979). The continuous periodic curves exhibited in Mortell & Seymour (1979) are KAM surfaces for the standard mapping.

Discontinuous solutions of equations (2.9)–(2.11) in the linear resonance region, $0 \leqslant \Delta \leqslant \Delta_l(A)$, were constructed in Seymour & Mortell (1980). These correspond to

gas motions containing shocks when the piston frequency is in the neighbourhood of a linear resonant frequency. The linear resonance region is characterized by the property that there is always an amplitude of the propagating signal which completes one cycle in the tube in an integer multiple of the period of H.

In this paper we construct discontinuous solutions of equations (2.9)–(2.11) in the *quadratic resonance region*, $\Delta_q(A) \leqslant \Delta \leqslant \frac{1}{2}$, of figure 1, which is defined by the property that there is always an amplitude of the propagating signal which completes *two* cycles in the tube in an odd multiple of the period of H. A mathematical definition of $\Delta_q(A)$ is given by equations (4.7), (4.10) and (4.13).

The linear and quadratic resonance regions are best described by writing equation (2.9) as the product of two mappings:

$$S:(s, F(s)) \rightarrow (\eta, \hat{F}(\eta)), \tag{2.12}$$

where $$\hat{F}(\eta) = F(s), \quad \eta = s + F(s);$$

$$P:(\eta, \hat{F}(\eta)) \rightarrow (\eta, F(\eta)), \tag{2.13}$$

where $$F(\eta) = \hat{F}(\eta) + H(\eta).$$

S is the 'simple wave mapping', measuring the accumulated distortion over a traversal of the tube, while P represents the effect of the input of the piston motion. A given function is a solution of equation (2.9) if it maps onto itself under the product PS. It was shown in Seymour & Mortell (1980) that solutions in the linear resonance region can be constructed by using the fixed points of the mapping PS. The linear resonance region contains those values of A and Δ for which the mapping PS has a fixed point. The quadratic resonance region contains those values of A and Δ for which the mapping $(PS)^2$ has a fixed point. Thus different resonance regions in the A–Δ plane can be characterized by the existence of fixed points of the mapping $(PS)^n$. Inside the transition curve of figure 1 (where the solutions are continuous) there are no fixed points of the mapping $(PS)^n$ for any n. Hence it is appropriate when considering the quadratic resonance region to work with the functional equation $(PS)^2$. Physically, this is equivalent to following a propagating wavelet through two cycles in the tube, when the equations connecting F at successive reflections from $x = 1$ at times $s\omega^{-1}$, $r\omega^{-1}$ and $\eta\omega^{-1}$ are

$$F(\eta) = F(r) + H(\eta), \quad \eta = r + F(r), \tag{2.14}$$

and $$F(r) = F(s) + H(r), \quad r = s + F(s). \tag{2.15}$$

We now introduce the new dependent variable

$$Z(y) = F(y) - \tfrac{1}{2}H(y) - \tfrac{1}{2}. \tag{2.16}$$

This choice is motivated by the fact that the fixed points of the mapping $(PS)^2$ occur at the zeros of Z. We also note that $F(y) = \frac{1}{2}H(y) + \frac{1}{2}$ is the solution of the linearized equations for $\omega = \Omega_n$, when, like $\sin(2\pi\eta)$, $H(\eta + \frac{1}{2}) = -H(\eta)$. (Note the contrast with linear resonance, $\omega = \omega_n$, where a periodic solution does not exist within linear theory.) Writing equations (2.14) and (2.15) in terms of Z and eliminating $Z(r)$ yields the functional equation

$$\left.\begin{aligned} Z(\eta) &= Z(s) + \tfrac{1}{2}H(\eta) + \tfrac{1}{2}H(s) + H(r), \\ \eta &= s + 2Z(s) + H(s) + H(r), \\ r &= \tfrac{1}{2} + s + Z(s) + \tfrac{1}{2}H(s), \end{aligned}\right\} \tag{2.17}$$

which corresponds to the mapping $(PS)^2$.

The problem of solving the governing nonlinear partial differential equations of periodic gas motions with frequencies in the quadratic-resonance region has been reduced to finding solutions $Z(\eta)$ of the equation (2.17) subject to the mean condition (2.10) on $F(\eta)$. Once $Z(\eta)$ is constructed, p and u can be found from equations (2.1), (2.2), (2.5), (2.8) and (2.16).

3. Construction of multi-valued invariant curves

We refer to a curve which is mapped onto itself by the equations (2.17) as an *invariant curve*. The key to constructing invariant curves lies in recognizing that *a fixed point of an invariant curve is analogous to a critical point of an ordinary differential equation*. This observation was exploited in Seymour & Mortell (1980) to construct invariant curves in the linear resonance region.

A fixed point (η_c, Z_c) of an invariant curve is defined by

$$\eta = s = \eta_c \quad \text{when} \quad Z(\eta) = Z(s) = Z_c. \tag{3.1}$$

For equations (2.17), the fixed points are located at the roots, η_c and r_c, of

$$H(\eta) + H(r) = 0, \quad \eta = r - \tfrac{1}{2} + \tfrac{1}{2}H(r), \quad Z(\eta) = 0. \tag{3.2}$$

The result that $Z_c = 0$ is one reason for the introduction of $Z(\eta)$ through equation (2.16). We take H to have the symmetry

$$H(y) = -H(y + \tfrac{1}{2}), \tag{3.3}$$

like the sinusoidal piston velocity used in experiments. Then the location of the fixed points has a simple geometric construction, and equations (3.2) become

$$H(\eta) = H(t), \quad t = \eta + \tfrac{1}{2}H(\eta), \quad Z(\eta) = 0, \tag{3.4}$$

where $t = r - \frac{1}{2}$. Note that $\hat{H}(\eta) = H(t(\eta))$ is the distortion of $H(\eta)$ under the simple wave map $t = \eta + \frac{1}{2}H(\eta)$. The construction for finding the critical points η_c and the corresponding $t_c = r_c - \frac{1}{2}$ is given in figure 2. The four distinct fixed points per period are located at $\eta_c = 0, \frac{1}{2}$, where $t_c = \eta_c$, and at $\eta_c = \eta_1, \eta_2$, where $0 < \eta_1 < \frac{1}{4}$, $\frac{3}{4} < \eta_2 < 1$. We note that $\eta_1 + \eta_2 = 1$, that η_1 and $t_1 (= \eta_1 + \frac{1}{2}H(\eta_1))$ tend to $\frac{1}{4}$, and that η_2 and $t_2 (= \eta_2 + \frac{1}{2}H(\eta_2))$ tend to $\frac{3}{4}$ as $A \to 0$. As $A \to \infty$, $\eta_1 \to 0$, $\eta_2 \to 1$ and t_1, $t_2 \to \frac{1}{2}$. By the symmetry of H, $r_1 = \eta_2$, $r_2 = \eta_1$ and $H(\eta_1) = -H(\eta_2)$. An alternative method for determining η_1 and η_2 is given in §4.2.

A fixed point of equations (2.17) may be interpreted physically as a *resonating wavelet* in the propagating signal carrying the value $Z = 0$. Thus, a resonating wavelet carries a value of $f = f_c$ such that

$$f_c = \frac{1}{2\omega M}(\tfrac{1}{2} - \Delta) + \tfrac{1}{2}h(\eta_c). \tag{3.5}$$

A solution containing a fixed point describes a signal which contains at least one amplitude, $f = f_c$, which completes two cycles in the tube in an odd multiple of the piston period. (A calculation which exhibits this is given at the end of §4.2.) The mathematical significance of a fixed point is that the local structure of the solutions of the functional equation (2.17), near the fixed point, can be described by an ordinary

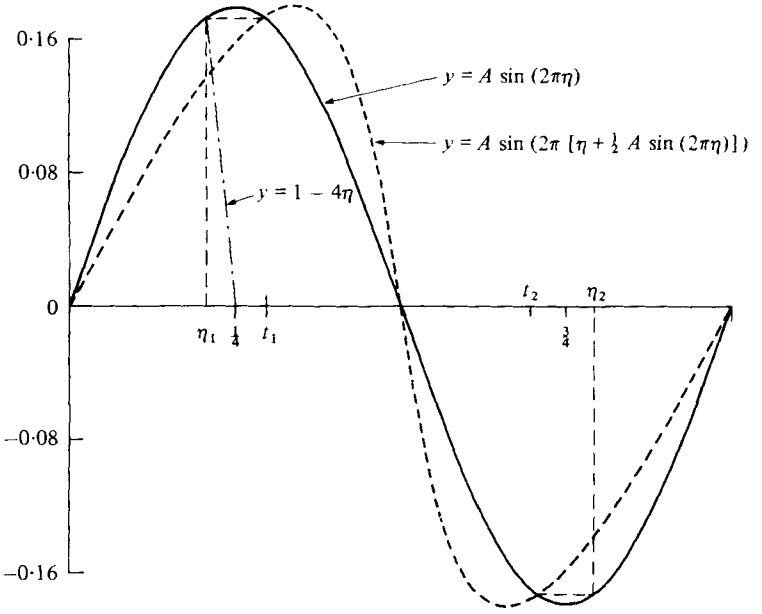

FIGURE 2. Location of fixed points of equation (2.17) using both equations (3.4) and (4.14). ——, $y = A \sin 2$; - - - - -, $y = A \sin(2\pi[\eta + \frac{1}{2}A \sin(2\pi\eta)])$; –·–·–, $y = 1 - 4\eta$.

differential equation. When $H(\eta)$ and $H(r)$ are expanded about $\eta = \eta_c$ and equations (2.17) and (3.2) are used, we obtain

$$H(\eta) = H(\eta_c) + \mu_1(1 + \mu_1 + a_1\mu_2)y + 2\mu_1 a_2 Z + O(y^2, Z^2) \tag{3.6}$$

and

$$H(r) = -H(\eta_c) + a_1\mu_2 y + \mu_2 Z + O(y^2, Z^2),$$

where $\mu_1 = H'(\eta_c)$, $\mu_2 = H'(r_c)$, $a_i = 1 + \frac{1}{2}\mu_i$ and $y = \eta - \eta_c$. Then the first of equations (2.17) yields the differential equation

$$\frac{dZ}{dy} = \frac{Z + a_1 y}{cZ + y}, \tag{3.7}$$

where $c = 2a_2(\mu_1 + a_1\mu_2)^{-1}$, to describe the behaviour of the functional equation (2.17) near $\eta = \eta_c$ and $Z = 0$. The critical points $\eta_c = \eta_1, \eta_2$, where $\mu_1 = \mu_2 > 0$, correspond to *saddle points* (or hyperbolic points).

The saddle points are the key to the construction of invariant curves of equations (2.17). There are four solution curves emanating from each saddle point (two positive and two negative) and in general two saddle points per period in the quadratic resonance region. The eight possible solution curves in the interval $[\eta_1, \eta_1 + 1]$ are labelled $Z^{\pm}_{1,2}(\eta)$, $W^{\pm}_{1,2}(\eta)$ with, for example, Z_2^+ and W_2^+ being the positive solutions leaving $(\eta_2, 0)$, Z_2^+ with positive slope and W_2^+ with negative slope (see figure 3). Differentiation of equations (2.17) with respect to s and setting (η, s, r) to their respective values corresponding to η_1 or η_2 gives

$$\frac{dZ(\eta_i)}{d\eta} = \pm\left(\frac{a_1}{c}\right)^{\frac{1}{2}}, \quad i = 1, 2, \tag{3.8}$$

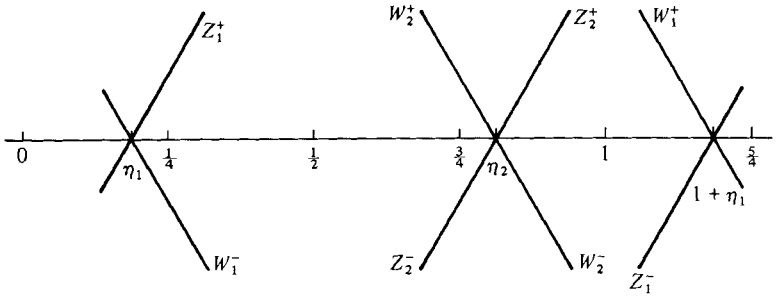

FIGURE 3. Diagram to illustrate the notation for solutions emanating from the fixed points of equation (2.17).

as the two possible slopes. Then it follows that

$$\frac{dZ_2^+(\eta_2)}{d\eta} = -\frac{dW_2^+(\eta_2)}{d\eta}. \tag{3.9}$$

The result (3.8) also follows from equation (3.7). Similarly, by repeated differentiation of equations (2.17) with respect to s, the higher derivatives of $Z(\eta)$ at a saddle point can be calculated. Hence the Taylor approximation to an invariant curve in the neighbourhood of a saddle point can be computed to any accuracy. This procedure provides an initial segment containing a saddle point which may then be extended using the exact mapping (2.17). The only error introduced is in the truncation of the Taylor series. This technique was introduced in Seymour & Mortell (1980) for the simpler functional equation describing flows in the linear resonance region, when there is usually only one saddle point per period.

It can be shown that, if $Z = \phi(\eta)$ is a solution of equations (2.17), then so is $Z = -\phi(\eta)$. As $H(\eta)$ has the symmetry (3.3), the eight solutions $Z_{1,2}^{\pm}(\eta)$, $W_{1,2}(\eta)$ can all be written in terms of the two curves $Z_1^+(\eta)$ and $Z(\eta)$ as follows:

$$\left.\begin{aligned} Z_1^-(\eta) &= -W_1^+(\eta) = -Z_2^+(2-\eta), && \eta \leqslant \eta_1+1,\\ Z_2^-(\eta) &= -W_2^+(\eta) = -Z_1^+(1-\eta), && \eta \leqslant \eta_2,\\ W_1^-(\eta) &= -Z_1^+(\eta), && \eta \geqslant \eta_1,\\ \text{and}\quad W_2^-(\eta) &= -Z_2^+(\eta), && \eta \geqslant \eta_2. \end{aligned}\right\} \tag{3.10}$$

The calculations of $Z_{1,2}^+(\eta)$ are independent in the sense that equations (2.17) map $Z_1^+(\eta)$ onto itself and also map $Z_2^+(\eta)$ onto itself. Figure 4 shows typical positive solution curves $Z_{1,2}^+(\eta)$ for $H(\eta) = A\sin(2\pi\eta)$ when $A = 0{\cdot}008$ and $A = 0{\cdot}08$.

The structure of the solution curves depends strongly on the magnitude of the similarity parameter A. Note that, as $A \to 0$, $\eta_2 \to \eta_1 + \frac{1}{2}(=\frac{3}{4})$ and $Z_2^+(\eta) \to Z_1^+(\eta - \frac{1}{2})$, $\eta_2 \leqslant \eta \leqslant 1+\eta_1$; otherwise $\eta_2 > \eta_1 + \frac{1}{2}$ and $\max Z_2^+(\eta) > \max Z_1^+(\eta)$. When A is in the *small-rate range*, $0 < A < A_s \ll 1$, the curves $Z_i^{\pm}$ and $W_j^{\pm}$, $(i,j) = (1,2)$ and $(2,1)$, are indistinguishable. Then there are apparently two single-valued solutions, one positive and one negative, connecting consecutive saddle points. These are analogues of separatrices for ordinary differential equations. As A increases these curves become distinct for $A > A_s$. While there is no proof of the existence of $A_s > 0$, the curves are not distinguishable on a scale of physical interest until $A > 0{\cdot}1$.

When $A_s < A < A_f$, where A_f is approximately $1{\cdot}0$, we say A is in the finite rate range. For A in this range the curves $Z_{1,2}^+$ (and hence by equations (3.10) $Z_{1,2}^-$ and

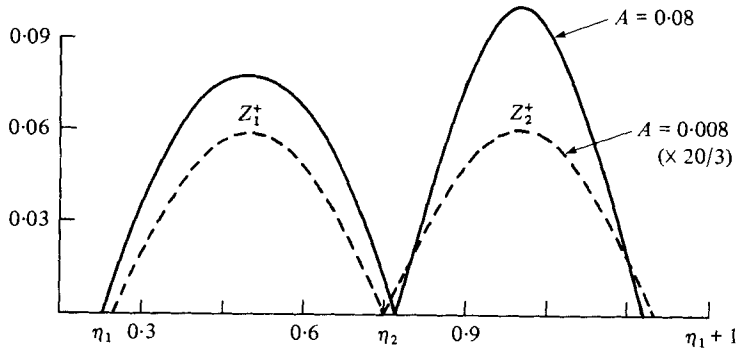

FIGURE 4. Solution curves $Z_1^+(\eta)$, $\eta_1(A) \leqslant \eta \leqslant \eta_2(A)$, and $Z_2^+(\eta)$, $\eta_2 \leqslant \eta \leqslant \eta_1 + 1$ of equation (2.17) when $A = 0{\cdot}008$ and $A = 0{\cdot}08$. The dashed curve ($A = 0{\cdot}008$) has been scaled by a factor 20/3.

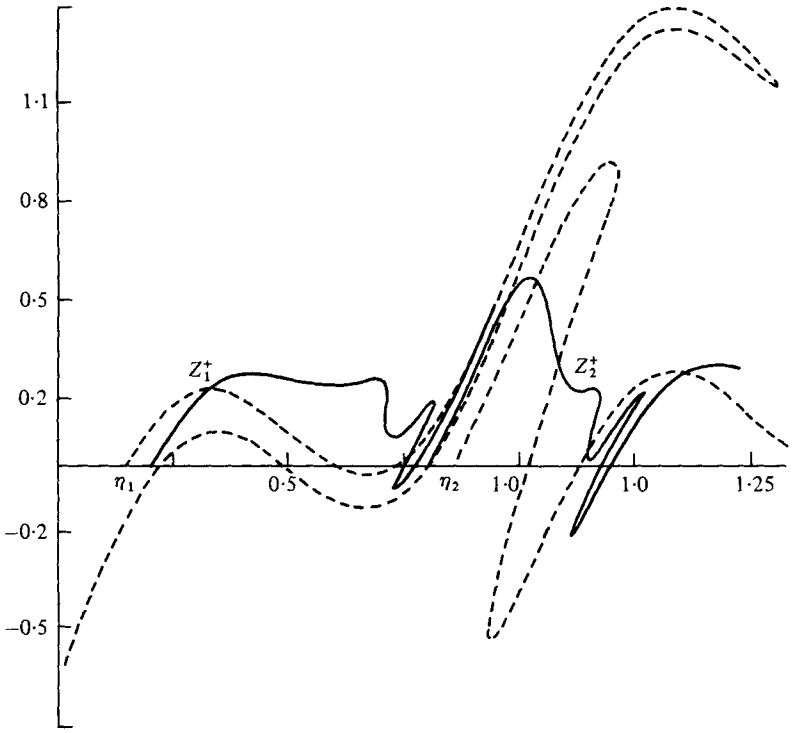

FIGURE 5. Multi-valued solution curves $Z_1^+(\eta)$, and $Z_2^+(\eta)$ of equation (2.17), for $A = 0{\cdot}2$ (—) and $A = 0{\cdot}5$ (- - -). The dashed curve has been scaled down by a factor 3.

$W_{1,2}^{\pm}$) are multi-valued. This is illustrated in figure 5 for $A = 0{\cdot}2$ and $A = 0{\cdot}5$, where it is seen that the size of the multi-valued loops increases with A. The mapping algorithm (2.17) is not affected by the multi-valuedness as it does not depend on derivatives of Z. Equations (2.15)–(2.17) imply that $Z(\eta)$ becomes multi-valued whenever

$$1 + F'(s) = 1 + Z'(s) + \tfrac{1}{2}H'(s) \to 0.$$

This corresponds to the 'breaking time' of some part of the propagating signal being

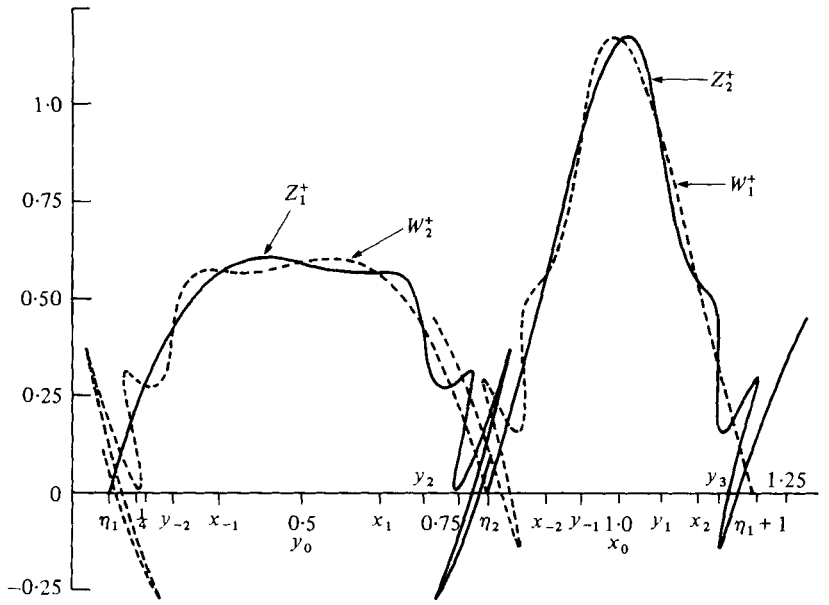

FIGURE 6. Multi-valued solution curves Z_1^+ and W_1^+ intersect on $\eta_1 \leqslant \eta \leqslant \eta_2$, Z_2^+ and W_1^+ intersect on $\eta_2 \leqslant \eta \leqslant \eta_1+1$, for $A = 0{\cdot}25$. The intersection point $(y_0, Z_1^+(y_0))$ maps onto $(y_2, Z_1^+(y_2))$ etc., and $(x_0, Z_2^+(x_0))$ maps onto $(x_2, Z_2^+(x_2))$ etc. under equation (2.17).

less than its travel time from $x = 1$ to $x = 0$ and back. Such a phenomenon cannot be described by a theory which assumes that waves propagate according to acoustic theory in which there is no distortion. The theories of quadratic resonance proposed by Galiev *et al.* (1970) and Keller (1975) both assume that waves in the tube propagate without distortion.

In the finite range the invariant curves $Z = Z_1^+(\eta)$ and $Z = W_2^+(\eta)$ (and similarly $Z = Z_2^+(\eta)$ and $Z = W_1^+(\eta)$) are distinct and intersect an infinite number of times on $[\eta_1, \eta_2]$. This is illustrated in figure 6 for $A = 0{\cdot}25$. The curve $Z_1^+(\eta)$ is intersected on $[\eta_1, \eta_2]$ by $W_2^+(\eta)$ and $Z_2^+(\eta)$ is intersected on $[\eta_2, \eta_1+1]$ by $W_1^+(\eta)$. The eight possible solution curves of equation (2.9) on $[\eta_1, \eta_1+1]$ are denoted by

$$F_{1,2}^{\pm} = Z_{1,2}^{\pm} + \tfrac{1}{2}H + \tfrac{1}{2} \quad \text{and} \quad G_{1,2}^{\pm} = W_{1,2}^{\pm} + \tfrac{1}{2}H + \tfrac{1}{2}. \tag{3.11}$$

The points of intersection at $y_0 = \frac{1}{2}$ and $x_0 = 1$ are recognized by noting that equations (3.10) imply that

$$F_1^+(\tfrac{1}{2}) = G_2^+(\tfrac{1}{2}) \quad \text{and} \quad F_1^+(1) = G_2^+(1), \tag{3.12}$$

as $H(\frac{1}{2}) = H(1) = 0$. Each generates a distinct sequence of intersection points on $[\eta_1, \eta_1+1]$,

$$(y_i, F^+(y_i)) \quad \text{and} \quad (x_i, F^+(x_i)), \quad -\infty < i < \infty, \tag{3.13}$$

under the mapping PS (equation (2.9)) and the periodicity of F. These are all of the intersection points on $[\eta_1, \eta_1+1]$, and the limit points of these sequences are the fixed points at $\eta = \eta_1, \eta_2$ and η_1+1. Thus, under the mapping PS, $F_1^+(\eta)$ maps onto $F_2^+(\eta)$ and vice versa, on noting the presence of $\frac{1}{2}$ in the definition (2.16). However, as equation (2.17) is derived by using equation (2.9) twice, $Z_1^+(\eta)$ and $Z_2^+(\eta)$ map onto themselves under the mapping $(PS)^2$. In fact, under $(PS)^2$, $(y_i, Z_j^+(y_i)) \to (y_{i+2}, Z_j^+(y_{i+2}))$

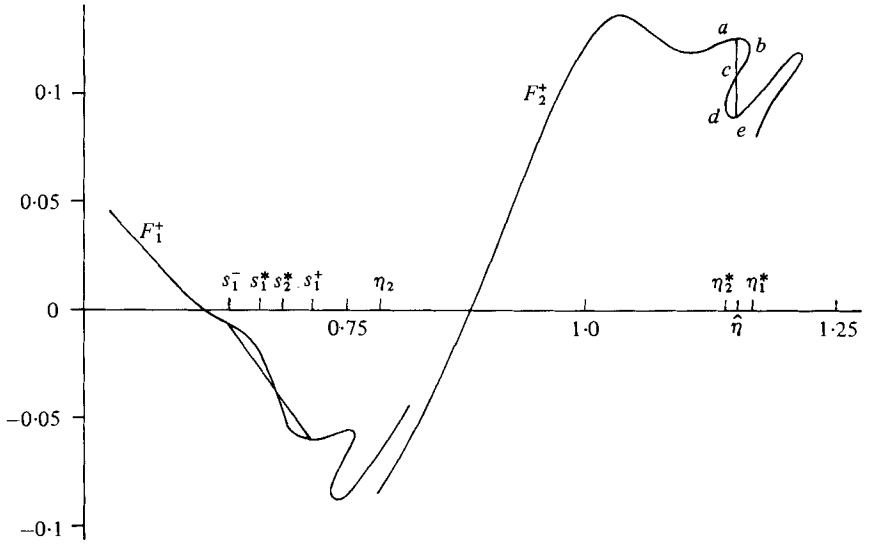

FIGURE 7. The continuous segment of $F_1^+(\eta)$, $s_1^- \leqslant \eta \leqslant s_1^+$, maps into the loop *abcde* in $F_2^+(\eta)$, $\eta_2^* \leqslant \eta \leqslant \eta_1^*$. A shock is inserted at η_s using the equal-area rule.

and $(x_i, Z_j^+(x_i)) \to (x_{i+2}, Z_j^+(x_{i+2}))$, $j = 1, 2$. In addition, it can be shown that the areas bounded by curves such as Z_1^+ and W_2^+, between successive points of intersection, are all equal, and their common value is

$$\int_{y_0}^{x_1} [W_2^+(\eta) - Z_1^+(\eta)]\, d\eta. \tag{3.14}$$

The proof of a similar result is given in Seymour & Mortell (1981).

4. Construction of discontinuous solutions

In the small-rate range there are two continuous separatrices connecting consecutive saddle points. In the finite range the equivalent curves through the saddle points are multi-valued. Here we show how single-valued, but discontinuous, separatrices are constructed from these. The locations of the discontinuities are determined by the 'equal area rule' for weak shocks. In both the small- and finite-rate ranges a composite of the separatrices is chosen to satisfy the mean condition (2.10) in the quadratic-resonance region. This introduces further shocks into the solution.

4.1. *Discontinuous separatrices*

It was shown in §3 that in the finite-rate range the curves $F_1^+(\eta)$ and $F_0^+(\eta)$ each have an infinite number of multi-valued loops. These must be made single-valued by inserting shocks to ensure the solutions are physically acceptable.

The multi-valued loop in $F_2^+(\eta)$ on $\eta_2^* \leqslant \eta \leqslant \eta_1^*$, illustrated in figure 7, is the image of $F_1^+(\eta)$ for $s_1^* \leqslant s \leqslant s_2^*$ under the mapping (2.9). The points of infinite slope of $F_2^+(\eta)$ at $\eta = \eta_1^*$ and η_2^* are the images of $F_1^+(s_1^*)$ and $F_1^+(s_2^*)$, where

$$dF_1^+(s_1^*)/ds = dF_1^+(s_2^*)/ds = -1, \quad \text{as} \quad d\eta/ds = 1 + F'(s).$$

A discontinuity is inserted in $F_2^+(\eta)$ at $\eta = \hat{\eta}$, $\eta_2^* \leqslant \hat{\eta} < \eta_1^*$. The points marked *a* and *e*

at $\eta = \hat{\eta}$ are the images of $F_1^+(s^-)$ and $F_1^+(s^+)$. They correspond to the amplitudes $F_1^+(s^-)$ and $F_1^+(s^+)$ which leave $x = 1$ at the distinct times $t = \omega^{-1}s^-$ and $t = \omega^{-1}s^+$ and return simultaneously at $t = \omega^{-1}\hat{\eta}$. Thus, by equation (2.9),

$$\hat{\eta} = s^- + F_1^+(s^-) = s^+ + F_1^+(s^+). \tag{4.1}$$

Equations (4.1) are equivalent to two of the weak-shock conditions (see Whitham 1974). The third condition is the equal-area rule, which, in the notation of § 2, becomes

$$\int_{s^-}^{s^+} F(s)\,ds - \tfrac{1}{2}(F(s^+) + F(s^-))\,(s^+ - s^-) = 0. \tag{4.2}$$

Using equations (2.9) and (4.1), the area enclosed by the loop *abcde* is

$$\int_{abcde} F_2^+(\eta)\,d\eta = \int_{s^-}^{s^+} F_1^+(s)\,ds - \tfrac{1}{2}(F_1^{+2}(s^-) - F_1^{+2}(s^+)) = 0, \tag{4.3}$$

by equations (4.1) and (4.2). Thus the weak-shock conditions imply that each multi-valued loop in $F_2^+(\eta)$ is made single-valued by inserting a discontinuity which cuts off lobes of equal area. We denote by $SF_2^+(\eta)$ the single-valued, but discontinuous, function derived from $F_2^+(\eta)$ by using the weak-shock conditions. The results of § 3 that the areas bounded by the curves $F_2^+(\eta)$ and $G_1^+(\eta)$ between the intersection points x_i and y_{i+1} and between y_{i+1} and x_{i+2} are equal implies that the associated shock lies in (x_i, x_{i+2}). Thus $SF_2^+(\eta)$ contains an infinite number of shocks in the interval $1 \leqslant \eta \leqslant \eta_1 + 1$. Similarly shocks are inserted to replace the multi-valued loops in $F_2^-(\eta)$ and $F_1^\pm(\eta)$ to give the functions SF_2^- and $SF_1^\pm$.

We must now check that these single-valued, discontinuous functions are solutions of equation (2.9), i.e. that $SF_1^+(\eta)$, $\eta_1 \leqslant \eta \leqslant \eta_2$, maps into $SF_2^+(\eta)$, $\eta_2 \leqslant \eta \leqslant \eta_1 + 1$, using equations (2.9) and (4.2), and vice versa. Alternatively, the function

$$F^+(\eta) = \begin{cases} SF_1^+(\eta), & \eta_1 \leqslant \eta \leqslant \eta_2, \\ SF_2^+(\eta), & \eta_2 \leqslant \eta \leqslant \eta_1 + 1, \end{cases} \tag{4.4}$$

must map onto itself using equations (2.9), (4.2) and periodicity. To show this we again break up equation (2.9) into the two mappings S and P. The simple wave mapping, S, is area preserving and, when it is applied to $F^+(\eta)$ and the equal-area rule is used, it yields a distorted function, $\hat{F}^+(\eta)$, with shocks of the same strengths and locations as $F^+(\eta)$. On noting that equation (2.9) may be written

$$F(\eta) = \hat{F}(\eta) + H(\eta), \tag{4.5}$$

and that the discontinuities of F^+ and $\hat{F}^+$ coincide in strength and location, clearly $F^+(\eta)$ maps into itself under equation (2.9) and hence is a discontinuous invariant curve. The function $F^-(\eta)$, $\eta_1 \leqslant \eta \leqslant \eta_1 + 1$, is constructed in a similar manner from $SF_1^-(\eta)$, $\eta_2 \leqslant \eta \leqslant \eta_1 + 1$, and $SF_2^-(\eta)$, $\eta_1 \leqslant \eta \leqslant \eta_2$.

Discontinuities may also be inserted in the curves $G_{1,2}^\pm(\eta)$ to make them single-valued. While a discontinuity introduced in $F_{1,2}^\pm(\eta)$ is compressional and is maintained, a discontinuity in $G_{1,2}^\pm(\eta)$ produces an expansion fan under the simple wave mapping. Hence the single-valued functions $SG_{1,2}^\pm(\eta)$ are not solutions of equation (2.9) and cannot be used. The direction of the jumps in the $F^\pm(\eta)$ curves is consistent with the entropy condition. The discontinuous separatrices $F^\pm(\eta)$ are illustrated in figure 8 for $A = 0{\cdot}3$.

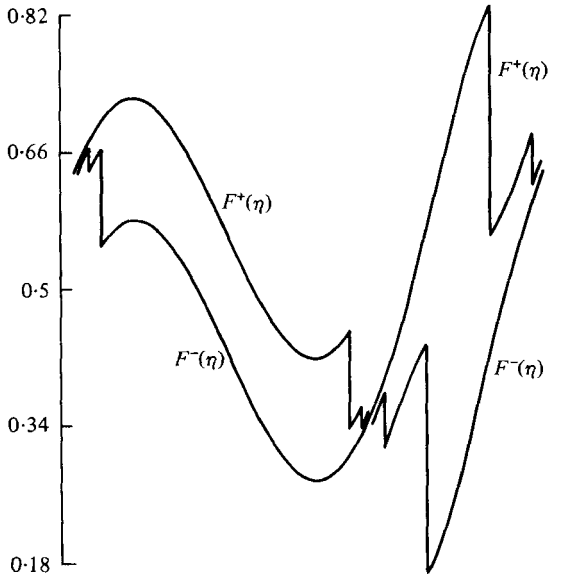

FIGURE 8. $F^{\pm}(\eta)$, $\eta_1 \leqslant \eta \leqslant \eta_2$, are separatrices of equation (2.9) corresponding to second-order fixed points, for $A = 0{\cdot}3$, which contain shocks.

4.2. *Quadratic resonance region*

In §§3 and 4.1 we have constructed continuous separatrices in the small-rate region and discontinuous separatrices in the finite-rate region. From these separatrices we have constructed the two functions $F^{\pm}(\eta)$, $\eta_1 \leqslant \eta \leqslant \eta_1 + 1$. Using equations (2.7) and (2.10), the functions $F^{\pm}(\eta)$ define the two frequencies

$$\omega^{\pm} = \Omega_n + \frac{1}{2}\int_{\eta_1}^{\eta_1+1} (F^{\pm}(\eta) - \tfrac{1}{2})\, d\eta. \tag{4.6}$$

A solution curve $F(\eta)$ of equation (2.9) which lies either above $F^+(\eta)$, and hence corresponds to a frequency $\omega > \omega^+$, or below $F^-(\eta)$, corresponding to $\omega < \omega^-$, does not contain a fixed point of the mapping $(PS)^2$ and hence the point in the A–Δ plane associated with F lies outside the quadratic-resonance region. Thus for a given value of A (and, hence, given $F^{\pm}(\eta)$) the frequencies $\omega^{\pm}$, calculated from equation (4.6), correspond to values of Δ at the edge of the quadratic resonance region. The boundary of the quadratic-resonance region for $0 \leqslant \Delta \leqslant \frac{1}{2}$ is given by

$$\Delta = \Delta_q(A) = 2(\omega^- - \omega_n), \tag{4.7}$$

and can be found from equation (4.6) by constructing the function $F^-(\eta)$ for various values of A. This procedure can be simplified by using the symmetries of the solutions. Defining

$$\mathscr{F}^{\pm}(\eta) = F^{\pm}(\eta) - \tfrac{1}{2}, \tag{4.8}$$

conditions (2.9), (3.3) and (4.2) imply that

$$\int_{\eta_1}^{\eta_2} \mathscr{F}^-(\eta)\, d\eta = \int_{\eta_2}^{\eta_1+1} \mathscr{F}^-(\eta)\, d\eta, \tag{4.9}$$

and that, by equation (3.10),

$$\int_{\eta_1}^{\eta_1+1} \mathscr{F}^-(\eta)\, d\eta = 4\int_{1}^{\eta_1+1} \mathscr{F}^-(\eta)\, d\eta. \tag{4.10}$$

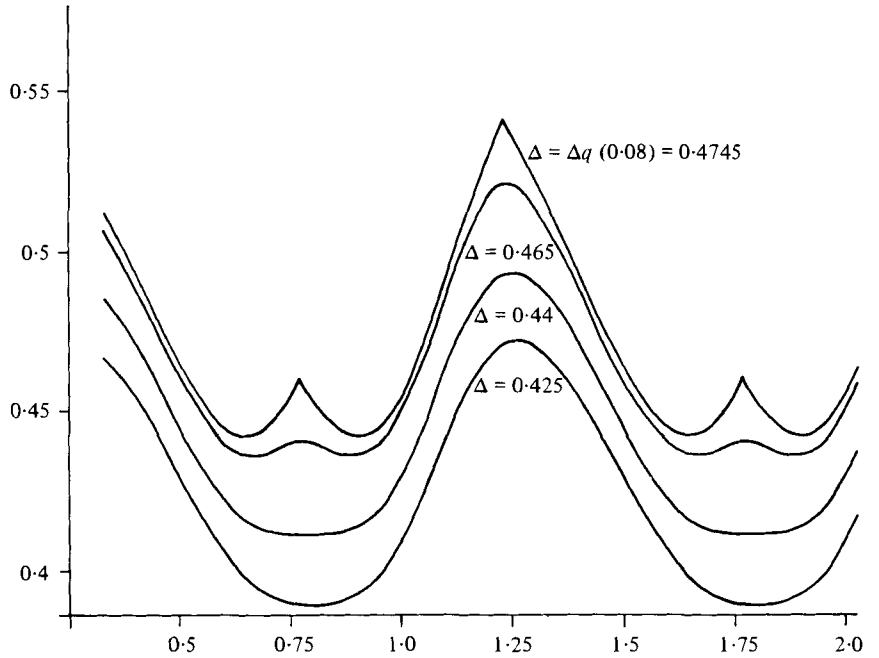

FIGURE 9. Solution curve of equation (2.17) for $A = 0{\cdot}08$ at the edge of the quadratic resonance region, $\Delta = 0{\cdot}4745$, with continuous periodic solution curves for $\Delta = 0{\cdot}465, 0{\cdot}44, 0{\cdot}425$.

Thus, by equations (4.6)–(4.8) and (4.10),

$$\Delta_q(A) = \tfrac{1}{2} + 4\int_1^{\eta_1+1} \mathscr{F}^-(\eta)\, d\eta. \tag{4.11}$$

Note that $\mathscr{F}^-(\eta) \leqslant 0$ and is continuous for $1 \leqslant \eta \leqslant \eta_1 + 1$, so that $\Delta_q(A) \leqslant \frac{1}{2}$, and $\Delta_q(A)$ can be calculated from equation (4.11) without the complications of shock fitting. The curve $\Delta = \Delta_q(A)$ is shown in figure 1.

In the small-rate range the curve $\Delta = \Delta_q(A)$ coincides with the transition curve separating the regions in the A–Δ plane corresponding to continuous and discontinuous periodic solutions of equations (2.9) and (2.10). Lying above F^+ and below F^- are continuous periodic curves which do not contain fixed points of the mapping (2.17). These curves were constructed in Mortell & Seymour (1979), where it was noted that in the small-rate range

$$\Delta_q(A) \simeq \tfrac{1}{2} - A\pi^{-1}.$$

Several continuous solutions, together with the limiting curve $F^-(\eta)$, are illustrated in figure 9 for $A = 0{\cdot}08$. The separatrix $F^-(\eta)$ yields $\Delta = \frac{1}{2} - 0{\cdot}0255$, on using equation (2.10), and hence for $A = 0{\cdot}08$ there are no continuous periodic solutions for $0{\cdot}4745 < \Delta \leqslant 0{\cdot}5$.

In the finite-rate range the edge of the quadratic-resonance region does not correspond to the transition from discontinuous to continuous solutions of equation (2.9). Any point in the region of the A–Δ plane bounded by the transition curve, the curve $\Delta = \Delta_l(A)$ and the curve $\Delta = \Delta_q(A)$ corresponds to a solution of equation (2.9) containing shocks. In principle, such solutions can be constructed by a procedure similar to that given in this paper by using higher-ordered fixed points of the mapping PS.

An alternative form for the locations of the critical points at η_1 and η_2 can be found by writing equation (4.9) in terms of $F^-(\eta)$. Then

$$\int_{\eta_2}^{\eta_1+1} F^+(\eta)\,d\eta - \int_{\eta_1}^{\eta_2} F^+(\eta)\,d\eta = \eta_1 - \eta_2 + \tfrac{1}{2}, \tag{4.12}$$

while equations (2.9), (2.16), (3.4) and (4.2) yield

$$\int_{\eta_2}^{\eta_1+1} F^+(\eta)\,d\eta - \int_{\eta_1}^{\eta_2} F^+(\eta)\,d\eta = \tfrac{1}{2}[F^{+2}(\eta_2) - F^{+2}(\eta_1)] = \tfrac{1}{2}H(\eta_2). \tag{4.13}$$

Then equations (4.12) and (4.13) imply that η_1 and η_2 are given by

$$H(\eta_1) = 1 - 4\eta_1 \quad \text{and} \quad H(\eta_2) = -H(\eta_1), \tag{4.14}$$

where

$$F(\eta_1) = 1 - 2\eta_1 \quad \text{and} \quad F(\eta_2) = 2\eta_1. \tag{4.15}$$

The simple forms (4.14) and (4.15) enable us to check the interpretation that a critical point corresponds to an amplitude which completes two cycles in the tube in unit time. We consider the signal $F(\eta_1)$, given by equation (4.15), which leaves $x = 1$ at $\eta = \eta_1$. Equations (2.7)–(2.9) then imply that the signal returns to $x = 1$ at $\eta = 1 + n - \eta_1$, and is reflected with amplitude $2\eta_1$, as required by equation (4.15). This signal subsequently returns to $x = 1$ at $\eta = 2n + 1 + \eta_1$ with amplitude, on reflection, equal to $1 - 2\eta_1$. This confirms the periodicity associated with critical points, and is most easily checked for the case $n = 0$ when $\omega = \frac{1}{4}$. The characteristic in x–t space emanating from a critical point is the 'everlasting characteristic' of Betchov (1958).

4.3. *Solution in the quadratic-resonance region*

The separatrices $F^{\pm}(\eta)$ in §4.1 are the solution curves corresponding to the applied frequencies $\omega = \omega^{\pm}$. As in Seymour & Mortell (1980) for the linear resonance region, solutions corresponding to frequencies in the range $\omega^- \leqslant \omega \leqslant \omega^+$, i.e. when

$$|\tfrac{1}{2} - \Delta| \leqslant \Delta_q(A), \tag{4.16}$$

are constructed by taking a composite of the separatrices to satisfy the mean condition (2.10). This introduces two further shocks into the solution, whose locations are uniquely determined by the mean condition.

It is now more convenient to work with $\mathscr{F}(\eta)$ and hence we define

$$\mathscr{F}(\eta) = \begin{cases} \mathscr{F}^+(\eta), & \eta_1 \leqslant \eta \leqslant x_s, \\ \mathscr{F}^-(\eta), & x_s \leqslant \eta < \eta_2, \\ \mathscr{F}^+(\eta), & \eta_2 \leqslant \eta < y_s, \\ \mathscr{F}^-(\eta), & y_s \leqslant \eta < \eta_1 + 1. \end{cases} \tag{4.17}$$

The direction of the shocks is again a consequence of the basic functional equation as discussed in §4.1. The shock locations, $x_s(\Delta)$ and $y_s(\Delta)$, are chosen to satisfy the mean condition (2.10). Integration of $\mathscr{F}(\eta)$ on $\eta_2 \leqslant \eta \leqslant \eta_1 + 1$ and use of equation (2.9) yields

$$\int_{\eta_2}^{\eta_1+1} \mathscr{F}(\eta)\,d\eta = \int_{\eta_1}^{\eta_2} \mathscr{F}(s)\,ds + \tfrac{1}{2}\{\mathscr{F}^2(\eta_2) - \mathscr{F}^2(\eta_1)\} - \left\{\int_{x^-}^{x^+} \mathscr{F}(s)\,ds - \tfrac{1}{2}[\mathscr{F}(x^+) + \mathscr{F}(x^-)]\,(x^+ - x^-)\right\}, \tag{4.18}$$

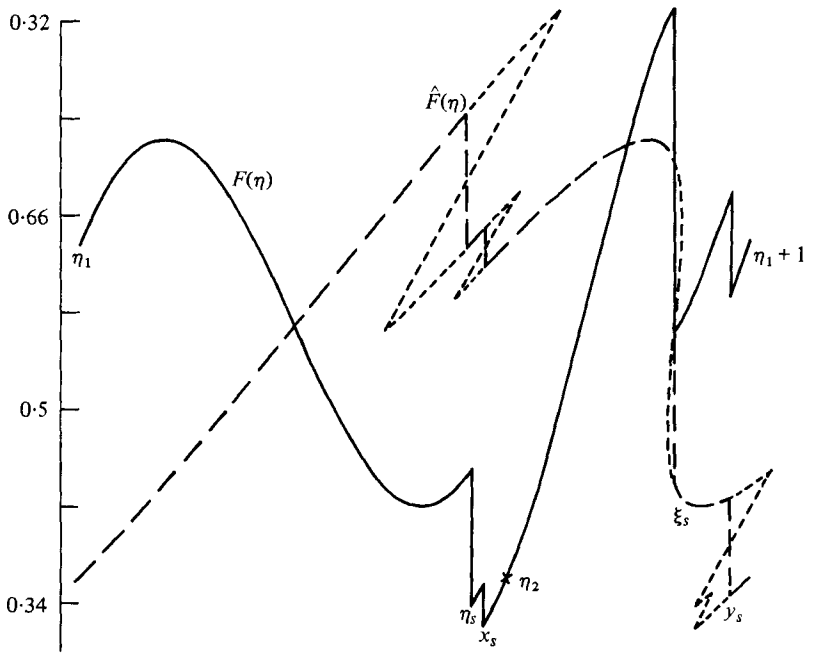

FIGURE 10. The solution of equation (2.9) $F(\eta)$ for $\eta_1 \leqslant \eta \leqslant \eta_1+1$ when $A = 0{\cdot}3$, $\Delta = 0{\cdot}57$ is the full curve. Shocks in the separatrices are at η_s and ξ_s, while shocks joining the separatrices are at x_s and y_s. The dashed curve, $\hat{F}(\eta)$, results from the application of the simple wave mapping (2.12) on $F(\eta)$.

where
$$y_s = x^+ + \tfrac{1}{2} + \mathscr{F}^-(x^+) = x^- + \tfrac{1}{2} + \mathscr{F}^+(x^-). \tag{4.19}$$

The equal-area rule, equations (2.10), and the definition (3.4) of the critical points at η_1 and η_2, imply that equation (4.18) reduces to

$$\int_{\eta_1}^{\eta_2} \mathscr{F}(\eta)\,d\eta = \int_{\eta_2}^{\eta_1+1} \mathscr{F}(\eta)\,d\eta = \tfrac{1}{2}(\tfrac{1}{2}-\Delta). \tag{4.20}$$

The condition (4.20) is a simple rule which uniquely determines the locations of the two shocks; for example

$$\begin{aligned} x_s(\tfrac{1}{2}) &= \tfrac{1}{2}, \quad y_s(\tfrac{1}{2}) = 1, \\ x_s(\Delta_q) &= \eta_2, \quad y_s(\Delta_q) = \eta_1+1, \\ x_s(-\Delta_q) &= \eta_1, \quad y_s(-\Delta_q) = \eta_2. \end{aligned}$$

It is easy to check that the discontinuous function $F(\eta)$, constructed by using equations (4.8) and (4.20), is a solution of equation (2.9) on using the equal area rule. This is illustrated in figure 10 for $A = 0{\cdot}30$, $\Delta = 0{\cdot}57$. For $\Delta = 0{\cdot}57$, the discontinuous separatrices contain shocks at η_s and ξ_s, while they are joined by shocks at x_s and y_s. The mapping (2.12) on F gives the function $\hat{F}$ which, on using the equal-area rule, has shocks at the above four locations. The shocks at η_s and x_s coalesce to give the shock at y_s; the shock at y_s maps into that at x_s; the shock at ξ_s maps into that at η_s while part of the continuous segment of $F(\eta)$ between η_1 and η_s breaks to form the shock at ξ_s. Recall that, by equation (2.13), the addition of $\hat{F}(\eta)$ and $H(y)$ then gives $F(\eta)$.

5. Discussion

Here we show that in the small-rate limit ($A \to 0$) the functional equation (2.17) reduces to a nonlinear ordinary differential equation. However, the shock strengths and their locations are not uniquely determined by the limiting differential equation. This contrasts with the functional equation which uniquely determines the full solution of the physical problem. We illustrate the finite-rate theory by exhibiting typical pressure variations on the piston and on the closed end. We point out the finite-rate features of the solutions presented and, finally, comment on the comparison of theory and experiment.

The small-rate approximation is found very simply by expanding the functional equation (2.17) for $|Z|, |H| \ll 1$ and retaining only quadratic terms. The resulting equation is

$$Z_0 Z_0' = -\tfrac{1}{4} H H', \tag{5.1}$$

on using the symmetry property $H(\eta + \frac{1}{2}) = -H(\eta)$ and the notation $Z \to Z_0$ as $A \to 0$. When H is given by equation (2.11) the critical points of equation (5.1) are located at $\eta_c = 0, \frac{1}{4}, \frac{1}{2}, \frac{3}{4}$. It was noted in §3 that the critical points of the functional equation (2.17) are at $\eta_c = 0, \eta_1, \frac{1}{2}, \eta_2$ and that $\eta_1 \to \frac{1}{4}$ and $\eta_2 \to \frac{3}{4}$ as $A \to 0$. The saddle points at $(\frac{1}{4}, 0)$ and $(\frac{3}{4}, 0)$ are connected by separatrices

$$z^{\pm}(\eta) = \pm \tfrac{1}{2} A \, |\cos(2\pi\eta)|. \tag{5.2}$$

(The curve $z^+(\eta)$ is similar to the dashed curve in figure 4 where $A = 0{\cdot}008$.) Thus from the mean condition (2.11), when

$$|\tfrac{1}{2} - \Delta| \geqslant \int_0^1 z^+(\eta)\, d\eta = \frac{A}{\pi} \equiv \tfrac{1}{2} - \Delta_s(A), \tag{5.3}$$

the solution curves of equation (5.1) are continuous and periodic. There are no continuous periodic solutions for $|\frac{1}{2} - A| < A/\pi$ and discontinuities connecting the separatrices $z^{\pm}(\eta)$ must be inserted. It was shown in Seymour & Mortell (1973) that the entropy and mean conditions uniquely determine the small rate solution in the linear resonance region. This is not so in the quadratic resonance region, and is vividly illustrated by considering the case $\Delta = \frac{1}{2}$. The 'solution' of equation (5.1),

$$Z_0(\eta) = \begin{cases} z^+(\eta), & \frac{1}{4} \leqslant \eta < \frac{1}{4} + \phi, \\ z^-(\eta), & \frac{1}{4} + \phi \leqslant \eta < \frac{3}{4}, \\ z^+(\eta), & \frac{3}{4} \leqslant \eta < \frac{5}{4} - \phi, \\ z^-(\eta), & \frac{5}{4} - \phi \leqslant \eta < \frac{5}{4}, \end{cases} \tag{5.4}$$

satisfies the entropy and mean conditions for any $0 \leqslant \phi \leqslant \frac{1}{2}$. In particular, when $\phi = 0, \frac{1}{2}$ the solutions are continuous. When equation (5.1) is viewed as the limit of the functional equation (2.17), then equation (4.20) implies that

$$\int_{\frac{1}{4}}^{\frac{3}{4}} Z_0(\eta)\, d\eta = \int_{\frac{3}{4}}^{\frac{5}{4}} Z_0(\eta)\, d\eta = \tfrac{1}{2}(\tfrac{1}{2} - \Delta), \tag{5.5}$$

and hence $\phi = \frac{1}{4}$ when $\Delta = \frac{1}{2}$. Alternatively, it can easily be checked that functions obtained by any other choice of y_s in equation (5.4) do not satisfy the mapping (2.9). The small-rate theory outlined above is equivalent to that given by Galiev *et al.* (1970) and Keller (1975).

On using the mean condition (5.5), the small-rate solution $Z_0(\eta)$ always contains two shocks at x_s and $y_s = X_s + \frac{1}{2}$, where x_s is given by

$$\sin(2\pi x_s) = \frac{1-2\Delta}{1-2\Delta_s(A)}. \tag{5.6}$$

These shocks are always of equal strength and a distance $\frac{1}{2}$ apart. In contrast, the solution (4.17) of the functional equation does not have these properties in general. This is illustrated in figure 10 for $A = 0{\cdot}3$, $\Delta = 0{\cdot}43$, where the shocks connecting the separatrices are at x_s, y_s with $y_s - x_s = 0{\cdot}36$. There is an additional shock at η_s in the separatrix $\mathscr{F}^+(\eta)$.

In the small-rate theory the signal propagates undistorted as in linear theory (although the signal shape is calculated from the nonlinear equation (5.1)). Hence the shock strength on the closed end is the same as that on the piston. This is not the case in the finite-rate theory, as is seen in figures 11 and 12. In figure 11 we compare the pressure on the piston calculated according to finite-rate theory, $P(\eta)$, and linear theory, $P_L(\eta)$, with the correction to linear theory in a regular expansion in the amplitude, $P_R(\eta)$, for $\epsilon = 0{\cdot}02$ and $\omega = 0{\cdot}74$ ($A = 0{\cdot}164$ and $\Delta = 0{\cdot}48$). The formulae for P, P_L and P_R are given in equations (6.7)–(6.10) of Mortell & Seymour (1979). Note that, as $\Delta \to \frac{1}{2}$, $P_L \to 0$ and $P_R \to \infty$, while P remains finite. $P(\eta)$ contains a shock of strength $0{\cdot}128$ at $x_s = 0{\cdot}413$ and a shock of strength $0{\cdot}208$ at $y_s = 0{\cdot}953$. For the same values of the physical parameters, figure 12 illustrates the corresponding pressures at the closed end, $x = 0$. The linear pressure $P_{L0}(\eta)$ is given by

$$P_{L0}(\eta) = \frac{A}{2\omega M}\left(\frac{\cos 2\pi\eta}{\sin \pi\Delta}\right), \tag{5.7}$$

while the second-order pressure, $P_{R0}(\eta)$, is given by

$$P_{R0}(\eta) = P_{L0}(\eta) + \frac{\pi A^2}{8\omega M}\cos(4\pi\eta)\left[\frac{1}{4\pi\omega} + \cot(4\pi\omega)\right]. \tag{5.8}$$

The pressure on the closed end, $P_0(\eta)$, calculated from the finite-rate theory is

$$P_0(\eta) = (\omega M)^{-1}[\Delta - F_0(\eta)], \tag{5.9}$$

where

$$F_0(\eta) = F(\theta), \quad \eta = \theta + \tfrac{1}{2}F(\theta) + \tfrac{1}{2}, \tag{5.10}$$

and F is the solution of equation (2.9) for $A = 0{\cdot}164$ and $\Delta = 0{\cdot}48$. $P_0(\eta)$ contains a shock of strength $0{\cdot}225$ at $x_s = 0{\cdot}684$ and a shock of strength $0{\cdot}231$ at $y_s = 1{\cdot}18$. We note that the shock strengths have changed owing to the distortion of the wave form in travelling from the piston to the closed end. This distortion arises through the transformation (5.10); acoustic propagation corresponds to $\eta = \theta + \frac{1}{2}$.

The pressure response curve, indicating maximum and minimum pressures and shock strengths on the closed end for the range of frequencies $0{\cdot}726 \leqslant \omega \leqslant 0{\cdot}777$ (about $\omega = \Omega_1$) and $\epsilon = 0{\cdot}02$ are illustrated in figure 13. For this amplitude and frequency range, A varies from $0{\cdot}158$ to $0{\cdot}181$. Figure 13 includes the maximum and minimum values of P_{R0}, P_0, and the values of the pressure at the top and bottom of each shock in P_0. For most frequencies in this range there are two shocks, but multiple shocks appear as the frequency approaches the edge of the quadratic resonance region. Then, for example, the shock with maximum T_2 and minimum B_2 splits into two shocks, the first from T_2 to B_3 and the second from T_3 to B_2.

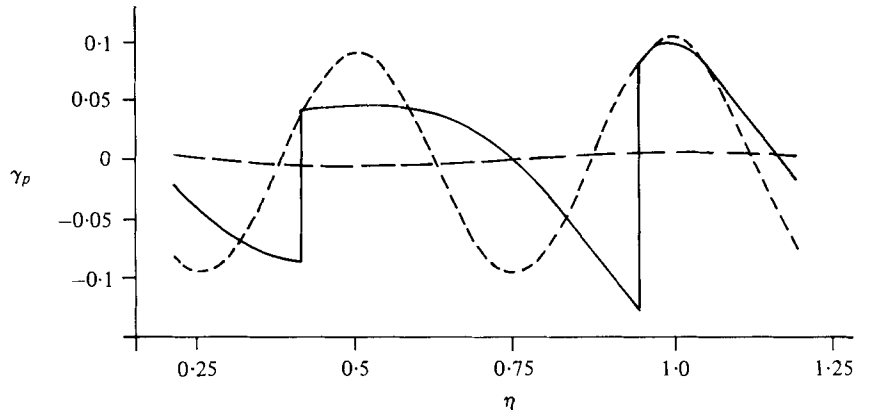

FIGURE 11. Pressure on the piston for $A = 0{\cdot}164$, $\omega = 0{\cdot}74$ (near Ω_1), corresponding to $\epsilon = 0{\cdot}02$. ——, present theory: – –, linear theory: - - - -, corrected linear theory.

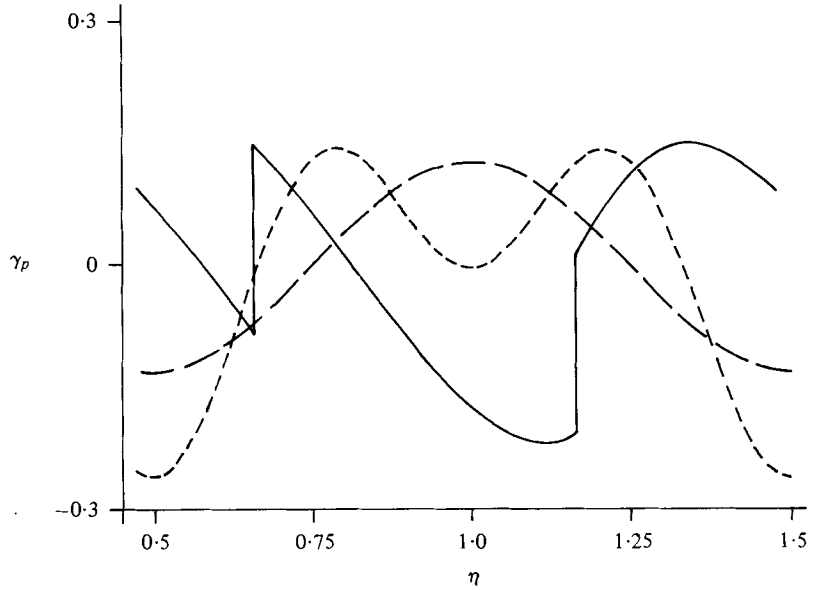

FIGURE 12. Pressure at the closed end for $A = 0{\cdot}164$, $\omega = 0{\cdot}74$ (near Ω_1), corresponding to $\epsilon = 0{\cdot}02$. ——, present theory: – – –, linear theory: - - - - -, corrected linear theory.

Pressure wave forms containing shocks have been observed for frequencies in the quadratic resonance region by Galiev *et al.* (1970) and Zaripov & Ilgamov (1976). Galiev *et al.* (1970) also gave a theoretical solution which extended the small-rate theory of Chester (1964) to the quadratic-resonance region. In our notation, they claim that there is an arbitrary phase shift between Z and $\frac{1}{2}H$ when constructing F from equation (2.16). (See their equation (2.7) *et seq.*) Their figure 4 corresponds to zero phase shift and agrees with the theory given here and that of Keller (1975). Their figure 5 results from introducing a phase shift of $\frac{1}{4}$ in the argument of $Z(\eta)$ (a shift of $\frac{1}{2}\pi$ in their notation) and seems to give better agreement with experiment than in figure 4. In our analysis there is no ambiguity about the phases and, indeed, their F,

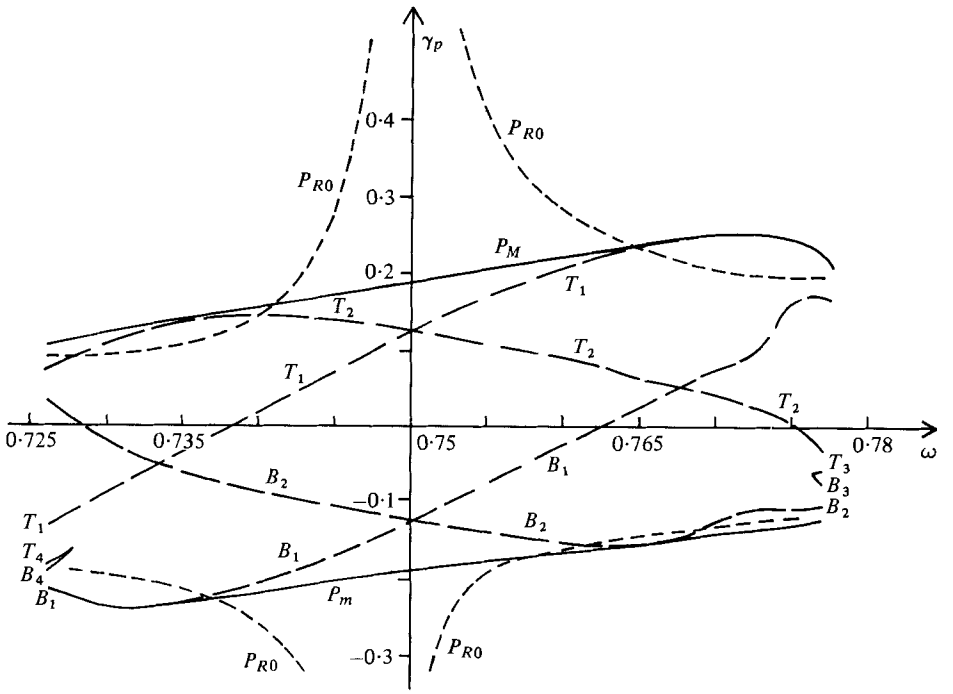

FIGURE 13. Pressure response curve at the closed end for $\epsilon = 0{\cdot}02$, $0{\cdot}726 \leqslant \omega \leqslant 0{\cdot}777$ (about $\omega = \Omega_1$). Curves indicate maximum pressure P_M; minimum pressure P_m; pressure at top and bottom of shocks $T_{1,2,3,4}$ and $B_{1,2,3,4}$; maximum and minimum pressures from P_{R0}.

as given by their equation (2.13) with a phase shift of $\frac{1}{2}\pi$, does not satisfy their equation (2.12).

The authors thank Mr Wolfgang Richter for his programming assistance. This work was supported in part by the Natural Sciences and Engineering Research Council of Canada under Grant A 9117. One of the authors (B.R.S.) acknowledges an S.R.C. Senior Visiting Fellowship at the University of Oxford.

REFERENCES

BETCHOV, R. 1958 Nonlinear oscillations of a column of gas. *Phys. Fluids* **1**, 205–212.

CHESTER, W. 1964 Resonant oscillations in closed tubes. *J. Fluid Mech.* **18**, 44–64.

CHIRIKOV, B. V. 1979 A universal instability of many-dimensional oscillator systems. *Phys. Rep.* **52**, 263–379.

GALIEV, S. U., ILGAMOV, M. A. & SODYKOV, A. V. 1970 Periodic shock waves in a gas. *Isz. Akad. Nauk S.S.S.R. Mech. Zhid. i Gaza* **2**, 57–66.

GREENE, J. M. 1979 A method for determining a stochastic transition. *J. Math. Phys.* **20**, 1183–1201.

KELLER, J. J. 1975 Subharmonic non-linear acoustic resonances in closed tubes. *Z. angew. Math. Phys.* **26**, 395–405.

MORTELL, M. P. & SEYMOUR, B. R. 1979 Nonlinear forced oscillations in a closed tube: continuous solutions of a functional equation. *Proc. Roy. Soc.* A **367**, 253–270.

MORTELL, M. P. & SEYMOUR, B. R. 1980 A simple approximate determination of stochastic transition for the standard mapping. *J. Math. Phys.* **21**, 2121–2123.

MOSER, J. 1962 *Nachr. Akad. Wiss., Göttingen, Math. Phys. Kl.* **1**, 1.

NAYFEH, A. H. & MOOK, D. T. 1979 *Nonlinear Oscillations.* Wiley-Interscience.

SEYMOUR, B. R. & MORTELL, M. P. 1973 Resonant acoustic oscillations with damping: small rate theory. *J. Fluid Mech.* **58**, 353–373.

SEYMOUR, B. R. & MORTELL, M. P. 1980 A finite-rate theory of resonance in a closed tube: discontinuous solutions of a functional equation. *J. Fluid Mech.* **99**, 365–382.

SEYMOUR, B. R. & MORTELL, M. P. 1981 Discontinuous solutions of a measure-preserving mapping. *SIAM J. Appl. Math.* **40**, 94–106.

WHITHAM, G. B. 1974 *Linear and Nonlinear Waves.* Wiley-Interscience.

ZAREMBO, L. K. 1967 Forced vibrations of finite amplitude in a tube. *Sov. Phys. Acoust.* **13**, 257–258.

ZARIPOV, R. G. & ILGAMOV, M. A. 1976 Nonlinear gas oscillations in a pipe. *J. Sound Vib.* **46**, 245–257.